CONSTRAINTS ON THE NEUTRON STAR AND INNER ACCRETION FLOW IN SERPENS X-1 USING NUSTAR

J. M. MILLER[1], M. L. PARKER[2], F. FUERST[3], M. BACHETTI[4,5], D. BARRET[4,5], B. W. GREFENSTETTE[3], S. TENDULKAR[3], F. A. HARRISON[3], S. E. BOGGS[6], D. CHAKRABARTY[7], F. E. CHRISTENSEN[8], W. W. CRAIG[9,10], A. C. FABIAN[2], C. J. HAILEY[10], L. NATALUCCI[11], F. PAERELS[10], V. RANA[3], D. K. STERN[12], J. A. TOMSICK[6], W. W. ZHANG[13]
Submitted to ApJL

ABSTRACT

We report on an observation of the neutron star low-mass X-ray binary Serpens X-1, made with *NuSTAR*. The extraordinary sensitivity afforded by *NuSTAR* facilitated the detection of a clear, robust, relativistic Fe K emission line from the inner disk. A relativistic profile is required over a single Gaussian line from any charge state of Fe at the 5σ level of confidence, and any two Gaussians of equal width at the same confidence. The Compton back-scattering "hump" peaking in the 10–20 keV band is detected for the first time in a neutron star X-ray binary. Fits with relativistically–blurred disk reflection models suggest that the disk likely extends close to the innermost stable circular orbit (ISCO) or stellar surface. The best-fit blurred reflection models constrain the gravitational redshift from the stellar surface to be $z_{NS} \geq 0.16$. The data are broadly compatible with the disk extending to the ISCO; in that case, $z_{NS} \geq 0.22$ and $R_{NS} \leq 12.6$ km (assuming $M_{NS} = 1.4\ M_\odot$ and $a = 0$, where $a = cJ/GM^2$). If the star is as large or larger than its ISCO, or if the effective reflecting disk leaks across the ISCO to the surface, the redshift constraints become measurements. We discuss our results in the context of efforts to measure fundamental properties of neutron stars, and models for accretion onto compact objects.

Subject headings: accretion, dense matter, equation of state, relativity, X-rays: binaries

1. INTRODUCTION

The equation of state of ultradense matter remains poorly known (see, e.g., Lattimer 2011). Such connditions cannot be replicated in terrestrial laboratories, leaving only astrophysical studies of neutron stars to solve this fundamental problem. The mass-radius relation for neutron stars depends sensitively on the equation of state of the ultradense stellar interior. Neutron star radius measurements are a particularly powerful discriminant, although extreme mass measurements can also help (e.g., Demorest et al. 2010). X-ray observations hold tremendous promise for radius measurement. Current instruments can easily measure thermal spectra from X-ray bursters (e.g., Guver et al. 2010) and quiescent X-ray transients (e.g., Guillot et al. 2013), although systematic uncertainties involving source distance, atmospheric modeling, and additional spectral components can complicate the extraction of reliable stellar radii (Boutloukos et al. 2010; Guver et al. 2012a, 2012b; Steiner et al. 2013).

[1] Department of Astronomy, The University of Michigan, 500 Church Street, Ann Arbor, MI 48109-1046, USA, jonmm@umich.edu

[2] Institute of Astronomy, The University of Cambridge, Madingley Road, Cambridge, CB3 OHA, UK

[3] Cahill Center for Astronomy and Astrophysics, California Institute of Technology, Pasadena, CA, 91125 USA

[4] Universite de Toulouse, UPS-OMP, Toulouse, France

[5] CNRS, Institut de Recherche en Astrophysique et Planetologie, 9 Av. colonel Roche, BP 44346, F-31028, Toulouse cedex 4, France

[6] Space Sciences Laboratory, University of California, Berkeley, CA 94720, USA

[7] Kavli Institute for Astrophysics and Space Research, Massachusetts Institute of Technology, 70 Vassar Street, Cambridge, MA 02139, USA

[8] Danish Technical University, Lyngby, DK

[9] Lawrence Livermore National Laboratory, Livermore, CA

[10] Columbia Astrophysics Laboratory and Department of Astronomy, Columbia University, 550 West 120th Street, New York, NY 10027, USA

[11] Istituto di Astrofisica e Planetologia Spaziali (INAF), Via Fosso del Cavaliere 100, Roma, I-00133, Italy

[12] Jet Propulsion Laboratory, California Institute of Technology, 4800 Oak Grove Drive, Pasadena, CA 91109, USA

[13] NASA Goddard Space Flight Center, Greenbelt, MD 20771, USA

Whenever an accretion disk is illuminated by an external source of hard X-rays, disk reflection is expected. The emergent reflection spectrum is shaped by Doppler shifts and gravitational redshifts; the extremity of these shifts can be used to measure the location of the inner disk with respect to the compact object (for a review, see Miller 2007; also see Miller et al. 2009). The most prominent parts of a disk reflection spectrum are the Fe K emission line and the Compton back-scattering "hump" that peaks between 10–30 keV. In principle, disk reflection spectrocopy has the potential to constrain the radius of a neutron star, since the disk must truncate at the surface, if not at larger radii (e.g. Cackett et al. 2008, 2010).

Spectra obtained with *XMM-Newton* and *Suzaku* have revealed potentially relativistic line shapes and have started to illustrate the power of disk reflection spectra to constrain the fundamental parameters of neutron stars (e.g. Bhattacharyya & Strohmayer 2007, Cackett et al. 2008, 2009, 2010; Di Salvo et al. 2009, Iaria et a. 2009, D' Ai et al. 2009, Papitto et al. 2009, Miller et al. 2011, Egron et al. 2013). A difficulty with X-ray CCD detectors is that pile-up can distort the shape of Fe K lines. Indeed, Ng et al. (2010) suggested that Fe K lines in neutron stars may actually be narrow and symmetric, and merely appear to be relativistic owing to pile-up distortions.

However, this possibility is not borne out by simulations (see, e.g., Miller et al. 2010), which instead suggest that pile-up acts to falsely narrow lines. Data obtained with gas spectrometers (e.g. Lin et al. 2010, Cackett et al. 2013), which do not suffer from photon pile-up, also point to broad lines, but such studies are clouded by low spectral resolution. Thus, uncertainties remain. The detection of a Compton back-scattering "hump" would also help to resolve the origin of Fe K lines in neutron stars, but no detection has previously been achieved.

Motivated by the ability of *NuSTAR* (Harrison et al. 2013) to reveal Fe K lines and broad-band disk reflection spectra in black holes (e.g. NGC 1365, GRS 1915+105, and Cygnus X-1; Risaliti et al. 2013, Miller et al. 2013, Tomsick et al. 2013),

free of photon pile-up distortions, we made a pilot observation of the well-known neutron star X-ray binary and "atoll" source Serpens X-1.

2. OBSERVATIONS AND DATA REDUCTION

NuSTAR observed Serpens X-1 twice on 12 and 13 July, 2013 (Sequence IDs 30001013002 and 30001013004). The data were screened and processed using the *NuSTAR* Data Analysis Software (NuSTARDAS) version 1.1.1, resulting in a total of 43.4 ks of on-target time. The source is relatively bright, so the net exposure after instrumental deadtime is taken into account is 30.4 ks. Spectra from the FPMA and FPMB detectors were extracted from 120" regions centered on the source position, using the "nuproducts" FTOOL. Corresponding response files appropriate for the pointing type (on-axis), source type (point), and extraction regions were also created. Backgrounds were created using the "nuskybgd" tool, which self-consistently accounts for background variations across the face of the detector.

The spectra were analyzed using XSPEC version 12.8 (Arnaud & Dorman 2000). The χ^2 statistic was used to measure the relative quality of different spectral models. Following Miller et al. (2013), "Churazov" weighting was employed in all fits to govern the influence of bins with significant but progressively less signal at high energy (Churazov et al. 1996). Errors are reported as the 1σ confidence level on all measurements. All fits were made assuming a neutral equivalent neutral hydrogen column density of 4.0×10^{21} cm^{-2} (based on Dickey & Lockman 1990), via the "tbabs" model, setting "vern" cross sections (Verner et al. 1996) and "wilm" abundances (Wilms et al. 2000).

3. ANALYSIS AND RESULTS

Serpens X-1 is known to exhibit Type-1 X-ray bursts at a rate of approximately 0.1 per hour (Galloway et al. 2008). Light curves were therefore created via the "nuproducts" tool and were searched for X-ray bursts; no bursts were detected. We also constructed an X-ray color–color diagram using energy selections typical of diagrams made using RXTE data, in order to provide the best correspondence. The *NuSTAR* observation was found to sample the usual "banana" branch rather than the "island" state or any other period of extreme or unusual behavior (see van der Klis 2006 for a description of atoll sources).

An initial inspection and comparison of the FPMA and FPMB spectra suggested that the source is confidently detected out to 40 keV. We therefore restricted subsequent spectral analysis to the 3–40 keV band. Initial fits revealed a striking agreement between the FPMA and FPMB spectra: when a constant was floated between the spectra to account for uncetainties in the flux calibration of the detectors, a value of 1.001 was measured. We therefore created a single combined total spectrum, background spectrum, and ancillary response matrix using the FTOOL "addascaspec". A single redistribution matrix file was created via "addrmf", weighting the single responses by their relative exposure times. The analysis described below pertains to the single combined spectrum.

A model consisting of a disk blackbody component ("diskbb", see Mitsuda et al. 1984), a simple single-temperature blackbody ("bbody"), and a power-law provides a good description of the time-averaged spectrum. This model can be interpreted fairly simply in terms of emission from the accretion disk, the stellar surface, and non-thermal emission that may arise through Comptonization and/or magnetic

processes. The simple blackbody may not represent direct emission from the stellar surface, nor from the entire surface. It may represent emission that has been modified by a boundary layer that can also be modeled via low–temperature, optically–thick Comptonization. However, that prescription is similar to a hot blackbody. Although this three-component model describes the continuum shape fairly well, it is not a formally acceptable fit: $\chi^2/\nu = 3282.8/919 = 3.57$ (also see Figures 1 and 2).

The fit is greatly improved when a relativistic line function is added: $\chi^2/\nu = 1010.9/912 = 1.11$ (see Figure 1). This model fits the line with the "kerrdisk" function (Brenneman & Reynolds 2006). This line model was employed because it allows for small changes to the spacetime induced by spin. The ISCO radius changes slowly for low values a, and neutron stars in X-ray binaries have low spin parameters ($a \leq 0.3$, where $a = cJ/GM^2$; see, e.g. Galloway et al. 2008, Miller, Miller, & Reynolds 2011).

We measure a disk blackbody temperature of $kT = 1.833(5)$ keV and a normalization of $K = 29.0(3)$, a simple blackbody temperature and normalization of $kT = 2.495(5)$ keV and $K = 0.0222(3)$, and a power-law index and normalization of $\Gamma = 3.41(3)$ and $K = 1.98(4)$ photons cm^{-2} s^{-1} at 1 keV. For "kerrdisk", we fixed outer emissivity index to equal the inner emissivity index, constrained the energy to the range possible for Fe (6.40–6.97 keV), and measured the line centroid energy, spin parameter, inclination, inner emission radius, and line flux. We measure a line centroid energy of $E = 6.97_{-0.01}$ keV (consistent with H-like Fe XXVI), an emissivity index of $q = 3.5(1)$, a spin parameter of $a = 0.17(2)$, an inner disk inclination of $i = 18(2)$ degrees, an inner radius of $r_{in} = 1.8(1)$ r_{ISCO} (10.6 ± 0.6 r_g), and a flux of 5.5×10^{-3} photons cm^{-2} s^{-1}. This flux translates into a line equivalent width of $W = 91(2)$ eV.

Fits with a relativistic line function are strongly required over a Gaussian model for the emission line. The best fits with the "kerrdisk" and "diskline" functions give $\chi^2/\nu = 1010.9/912$. Instead modeling the line with a Gaussian corresponding to any charge state of Fe (6.40–6.97 keV) gives $\chi^2/\nu = 1052.1/915$ (E = 6.53(2) keV, $\sigma = 0.44(2)$ keV). Via an F-test, a relativistic line function is therefore required at the 5.3σ level of confidence.

It is also possible to test whether or not the line profile is actually a composition of different plausible charge states. Adding two Gaussians from any charge state of Fe, constrained to have the same width but allowed to have different strengths, gives a significantly worse fit than a single relativistic line: $\chi^2/\nu = 1266.1/915$. This effectively eliminates the possibility that the line profile arises in any form of diffuse gas far from the stellar surface.

Using this phenomenological model, we measure an unabsorbed flux of 6.1×10^{-9} erg cm^{-2}s^{-1} in the 3.0–40.0 keV band, implying 1.5×10^{-8} erg cm^{-2}s^{-1} in the 0.5–40.0 keV band. The 3–40 keV range is closer to that common in X-ray monitors and corresponds to 0.2–0.3 Crab. The distance to Serpens X-1 is likely 7.7 ± 0.9 kpc (based on X-ray burst properties; see Galloway et al. 2008). A luminosity of $1.1(2) \times 10^{38}$ erg s^{-1} follows from the inferred 0.5–40.0 keV flux. It is likely that Serpens X-1 was accreting at a high fraction of its Eddington limit during our observation.

Figure 1 shows clear hallmarks of disk reflection, even after fitting the relativistic line, including an edge between 9–10 keV consistent with H-like Fe XXVI, and a flux excess

in the 10–20 keV range consistent with a Compton back-scattering hump. It is also clear in Figure 1 that most of the flux capable of ionizing Fe comes from the blackbody component. To self–consistently model the reflection, then, we employed a new version of the well–known "reflionx" model (Ross & Fabian 2005), wherein a blackbody illuminated the disk instead of the power-law.

The "kerrdisk" line model was replaced by "reflionx", convolved with the kernel of "kerrdisk", called "kerrconv". Its parameters include inner and outer disk emissivity indices (q_{out} was fixed to q_{in} in our fits), the inclination of the inner disk, the spin parameter of the compact object, and the inner and outer emitting radii (in units of the ISCO radius; $R_{out} = 400$ was fixed in all cases). The "reflionx" model variables include the ionization parameter of the disk ($\xi = L/nr^2$), the abundance of iron (A_{Fe}), the blackbody temperature (tied to that of the independent blackbody), and the flux.

Table 1 lists the results of models for the time-averaged spectrum of Serpens X-1, including relativistically–blurred disk reflection (Models 1–18). The spin of Serpens X-1 is unknown as kHz QPOs and burst oscillations have not been detected. For completeness we considered fits with three spin values: $a = 0.0, 0.12, 0.24$. The latter two values span the range of spin parameters implied in other "atoll" sources (see, e.g. Galloway et al. 2008), assuming $R_{NS} = 10$ km, $M_{NS} = 1.4\ M_\odot$, and $I_{NS} = (2/5)MR^2$ as per a simple sphere. Similarly, the iron abundance of Serpens X-1 is unknown, so we explored fits with three values (relative to solar): $A_{Fe} = 1.0, 2.0, 3.0$. Last, in order to test the sensitivity of the spectrum to the inner radius of the disk, we considered fits with variable inner radii, and fits with $r_{in} = 1.0\ r_{ISCO}$.

The best blurred reflection fits (Models 5, 11, 17) uniformly give significantly better fits than models without reflection: an F-test gives an $F = 96.3$, or a false-alarm probability of just 1.1×10^{-21}. Combined with the ability of the reflection models to naturally model the 10–20 keV flux excess in Figure 1, this signals that the full broad-band disk reflection spectrum has been detected in Serpens X-1.

All of the models in Table 1 prefer very low inclinations; this corresponds well with recent optical observations that independently point an inclination of 10° or less (Cornelisse et al. 2013). The results in Table 1 also clearly signal that the fits are largely insensitive to the spin parameter of the neutron star. This is consistent with expectations: even for $a = 0.24$, the ISCO radius only changes marginally to $r_{ISCO} = 5.89 r_g$ (where $r_g = GM/c^2$).

The data show a slight preference for an enhanced iron abundance in Serpens X-1. Given that the binary orbital period of Serpens X-1 appears to be just 2 hours (Cornelisse et al. 2013), it is possible that the companion is evolved or degenerate, skewing e.g. Fe/O abundance ratios. Enhanced abundances are partly degenerate with the normalization of the reflection component and its ionization. Excellent fits are achieved regardless of the abundance, however, and parameters of greater interest show no trend with abundance.

The models wherein the inner disk radius is allowed to float nominally prefer a radius that is slightly larger than the ISCO; however, the improvement in the fit statistic is not significant, and 90% and/or 3σ confidence errors include the ISCO radius. Fits to the time-averaged spectra may be characterized as being broadly consistent with a disk extending to the ISCO.

We also examined the broad flux trends within the observation, and identified a period of high flux for consideration

(see Figure 3). Total FPMA and FPMB spectra, background spectra, and responses were created for "GTI2" in exactly the same manner as for the time-averaged spectrum. The results of fits to this segment of the observation are also given in Table 1 (see Models 19–24).

Figure 4 shows plots of $\Delta\chi^2$ versus r_{in} for models 5 and 23, in order to illustrate the sensitivity of the spectra to the inner extent of the disk. Fits to the time-averaged (Model 5) and high-flux (Model 23) spectra point to a disk that hovers close to the ISCO. Model 5 prefers $r_{in} > r_{ISCO}$, but Model 23 suggests that $r_{in} = r_{ISCO}$ is fully compatible with the data. The disk continuum is less incisive than the reflection spectrum, but it can serve as a broad consistency check. The disk continua in Table 1 imply inner radii of 13–15 km (1.03–1.20 r_{ISCO} or 6.2–7.2 r_g for $M_{NS} = 1.4\ M_\odot$ and $a = 0$) for a canonical spectral hardening factor of 1.7 (Shimura & Takahara 1995).

For $a = 0$, the gravitational redshift implied by the fits is given by $z + 1 = 1/\sqrt{1 - 2GM/rc^2}$. The best models for the time-averaged spectra in Table 1 (e.g. Model 5) give $r = 1.3\ r_{ISCO} = 7.8\ r_g$. The neutron star must be smaller than the inner disk radius, giving a limit of $z_{NS} \geq 0.16$. Within the high flux interval, even smaller inner disk radii are preferred, and errors include $r = r_{ISCO}$. If the disk extends to the ISCO, $z_{NS} \geq 0.22$ and $R_{NS} \leq 12.6$ km assuming $M_{NS} = 1.4\ M_\odot$. The masses of neutron stars in low-mass X-ray binaries are not known precisely, but 1.4 $M_\odot$ is a reasonable average (Lattimer 2011). If the neutron star surface itself truncates the disk (and if any boundary layer is small in radial extent), or if the effective reflection radius extends within the ISCO, then these limits could be regarded as measurements.

4. DISCUSSION

We have analyzed an initial observation of the neutron star low-mass X-ray binary Serpens X-1. Owing to the abilities of *NuSTAR*, an Fe K line in the spectrum is revealed to be skewed at a high level of statistical confidence, and the Compton back-scattering "hump" expected in disk reflection scenarios is detected in a neutron star X-ray binary for the first time. Both findings are robust since the FPMA and FPMB detectors do not suffer from flux distortions due to effects such as photon pile-up. Clearly, broad Fe K lines in at least some neutron star X-ray binaries arise in the inner disk, and can be used to probe the stellar properties and inner accretion flow.

In contrast to black holes, an ISCO is not necessarily a feature of accretion onto neutron stars. The stellar radius could exceed its own ISCO, and/or the stellar magnetic field can truncate the disk at much larger radii. The latter is certainly the case in typical X-ray pulsars, but also in transient sources such as SAX J1808.4−3658 (Cackett et al. 2009) and IGR J17480−2446 in Terzan 5 (Miller et al. 2011). Fits to the robust data obtained with *NuSTAR* indicate that the disk likely extends to the ISCO, or hovers just above such a radius. The high luminosity implied during this observation makes it more likely that the disk is not impeded by a magnetic field; this is also indicated by fits to a high–flux interval of the observation.

If the neutron star radius in Serpens X-1 is small, this observation represents the strongest observational indication of an ISCO in a neutron star low-mass X-ray binary. In this case, our fits require $z_{NS} \geq 0.16$ (best fit), or $z \geq 0.22$ and $R_{NS} \leq 12.6$ km if $r = r_{ISCO}$, assuming $M_{NS} = 1.4\ M_\odot$. If the star in Serpens X-1 is larger than its ISCO, the disk may then be truncated by a the stellar surface and/or a thin boundary layer. It is also possible that material in the inner disk may

leak across the ISCO and be reflective between the ISCO and stellar surface. In either of these two scenarios, the limits placed by our fits may be characterized as measurements. Some equations of state may then be incompatible with our observations (see Lattimer 2011).

The statistically significant skewing of the line profile clearly signals that dynamics and gravitation close to the neutron star drive our results. However, the results are not entirely model–independent. A disk reflection spectrum is required by the data. Although we achieved excellent fits with "reflionx", different and/or future reflection and relativistic convolution models may yield slightly different results.

REFERENCES

Arnaud, K. A., and Dorman, B., 2000, XSPEC is available via the HEASARC on-line service, provided by NASA/GSFC

Bhattacharyya, S., & Strohmayer, T., 2007, ApJ, 64, L103

Boutloukos, S., Miller, M., Lamb, K., 2010, ApJ, 720, L15

Brenneman, L., & Reynolds, C. S., 2006, ApJ, 652, 1028

Cackett, E. M., Miller, J. M., Bhattacharyya, S., Grindlay, J. E., Homan, J., van der Klis, M., Miller, M. C., Strohmayer, T. E., Wijnands, R., 2008, ApJ, 674, 415

Cackett, E. M., Miller, J. M., Ballantyne, D. R., Barret, D., Bhattacharyya, S., Boutelier, M., Miller, M. C., Strohmayer, T. E., Wijnands, R., 2010, ApJ, 720, 205

Cackett, E. M., Miller, J. M., Reis, R., C., Fabian, A. C., Barret, D., 2012, ApJ, 755, 27

Churazov, E., Gilfanov, M., Forman, W., Jones, C., 1996, ApJ, 471, 673

Cornelisse, R., Casares, J., Charles, P. A., & Steeghs, D., 2013, MNRAS, 432, 1361

D'Ai, A., Iaria, R., Di Salvo, T., Matt, G., Robba, N. R., 2009, ApJ, 693, L1

Demorest, P. B., Pennucci, T., Ransom, S. M., Roberts, M. S., E., Hessels, J. W. T., 2010, Naure, 467, 1081

Diaz Trigo, M., Sidoli, L., Boirin, L., Parmar, A. N., 2012, A&A, 543, 50

Dickey, J. M., & Lockman, F., J., 1990, ARA&A, 28, 215

Di Salov, T., D'Ai, A., Iaria, R., Burderi, L., Dovciak, M., KAras, V., Matt, G., Papitto, A., Piraino, S., Riggio, A., Robba, N. R., Santangelo, A., 2009, MNRAS, 398, 2022

Egron, E., Di Salvo, T., Motta, S., Burderi, L., Papitto, A., Duro, R., D'Ai, A., Riggio, A., Belloni, T., Iaria, R., Robba, N., Paraino, S., Santangelo, A., 2013, A&A, 550, 5

Galloway, D. K., Muno, M. P., Hartman, J. M., Psaltis, D., Chakrabarty, D., 2008, ApJS, 179, 360

Guillot, S., Servaillat, M., Webb, N., Rutledge, R. E., 2013, ApJ, 772, 7

Guver, T., Ozel, F., Cabrera-Lavers, A., Wroblewski, P., 2010, ApJ, 712, 964

Guver, T., Psaltis, D., Ozel, F., 2012a, ApJ, 747, 76

Guver, T., Ozel, F., Psaltis, D., 2012b, ApJ, 747, 77

Harrison, F. A., et al., 2013, ApJ, 770, 103

Iaria, R., D'Ai, A., Di Salvo, T., Robba, N. R., Riggio, A., Papitto, A., Burderi, L., 2009, A&A, 505, 1143

Lattimer, J. M., 2011, Ap&SS, 336, 67

Lattimer, J. M., & Prakash, M., 2007, PhR, 442, 109

Lin, D., Homan, J., & Remillard, R. A., 2010, ApJ, 719, 1350

London, R. A., Taam, R. E., & Howard, W. M., 1986, ApJ, 306, 170

Magdziarz, P., & Zdziarski, A. A., 1995, MNRAS, 273, 837

Miller, J. M., 2007, ARA&A, 45, 441

Miller, J. M., Reynolds, C. S., Fabian, A. C., Miniutti, G., Gallo, L. C., 2009, ApJ, 697, 900

Miller, J. M., D'Ai, A., Bautz, M. W., Bhattacharyya, S., Burrows, D. N., Cackett, E. M., Fabian, A. C., Freyberg, M. J., Haberl, F., Kennea, J., Nowak, M. A., Reis, R. C., Strohmayer, T. E., Tsujimoto, M., 2010, ApJ, 724, 1441

Miller, J. M., Miller, M. C., & Reynolds, C. S., 2011, ApJ, 731, 5

Miller, J. M., Parker, M. L., Fuerst, F., Bachetti, M., Harrison, F. A., Barret, D., Boggs, S. E., Chakrabarty, D., Chistensen, F. E., Craig, W. W., Fabian, A. C., Grefenstette, B. W., Hailey, C. J., King, A. L., Stern, D. K., Tomsick, J. A., Walton, D. J., Zhang, W. W., 2013, ApJ, in press, arXiv:1308.4669

Mitsuda, K., Inoue, H., Koyama, K., Makishima, K., Matsuoka, M., Ogawara, Y., Suzuki, K., Tanaka, Y., Shibazaki, N., Hirano, T., 1984, PASJ, 36, 741

Ng, C., Diaz Trigo, M., Cadolle Bel, M., & Migliari, S., 2010, A&A, 522, 96

Papitto, A., Di Salvo, T., D'Ai, A., Iaria, R., Burderi, L., Riggio, A., Manna, M. T., & Robba, N. R., 2009, A&A, 493, L39

Risaliti, G., Harrison, F. A., Madsen, K. K., Walton, D. J., Boggs, S. E., Christensen, F. E., Craig, W. W., Grefenstette, B. W., Hailey, C. J., Nardini, E., Stern, D., Zhang, W. W., 2013, Nature, 494, 449

Reynolds, C. S., & Fabian, A. C., 2008, ApJ, 675, 1048

Ross, R. R., & Fabian, A. C., 2005, MNRAS, 358, 211

Shafee, R., McKinney, J. C., Narayan, R., Tchekhovskoy, A., Gammie, C. F., McClintock, J. E., 2008, ApJ, 687, L25

Shimura, T., & Takahara, F., 1995, ApJ, 445, 780

Steiner, A., Lattimer, J., Brown, E., 2013, ApJ, 765, L5

Tomsick, J., et al., 2013, ApJ, submitted.

van der Klis, M., 2006, in "Compact Stellar X-ray Sources", ed. W. H. G. Lewin & M. van der Klis (Cambridge University Press), 39

Verner, D. A., Ferland, G. J., Korista, K. T., & Yakovlev, D. G., 1996, ApJ, 465, 487

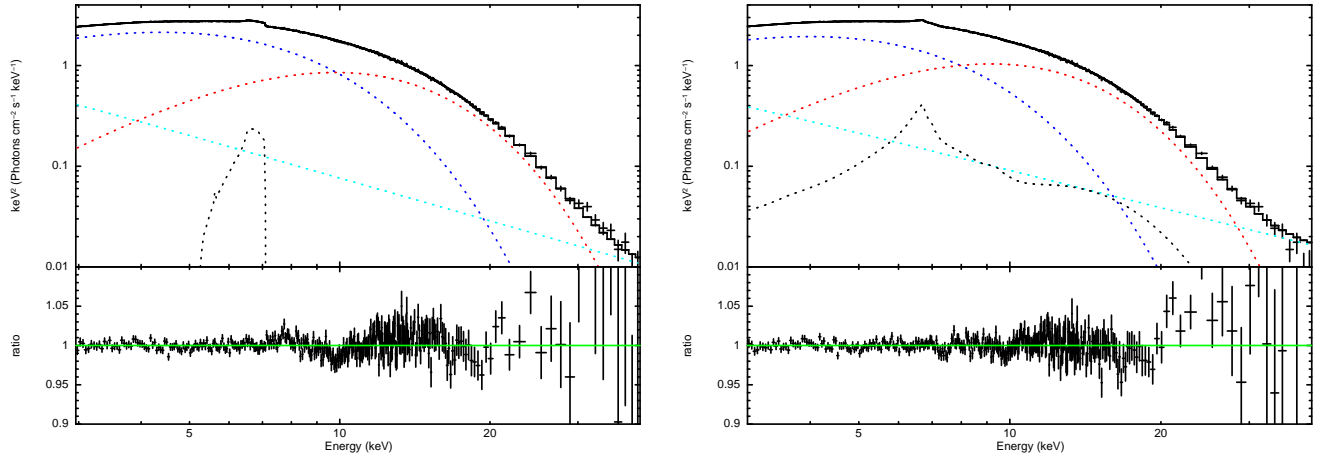Wilms, J., Allen, A., McCray, R., 2000, ApJ, 542, 914

FIG. 1.— The *NUSTAR* 3–40 keV spectrum of Serpens X-1 is shown above, with the FPMA and FPMB detectors combined. *Left*: The best-fit phenomenological spectral model is shown here. The model consists of disk blackbody (blue), simple blackbody (red), power-law (cyan), and relativistic disk line (black) components. The edge feature between 9–10 keV is consistent with the K edge of Fe XXVI, and the flux excess in the 10–20 keV band is consistent with the Compton back-scattering "hump" expected from disk reflection. *Right*: The best relativistically–blurred disk reflection fit (Model 5 in Table 1) is shown here. The line function has been replaced with a version of "reflionx" suited to blackbody illumination of the disk, and convolved with the "kerrconv" function. A significantly better fit is achieved.

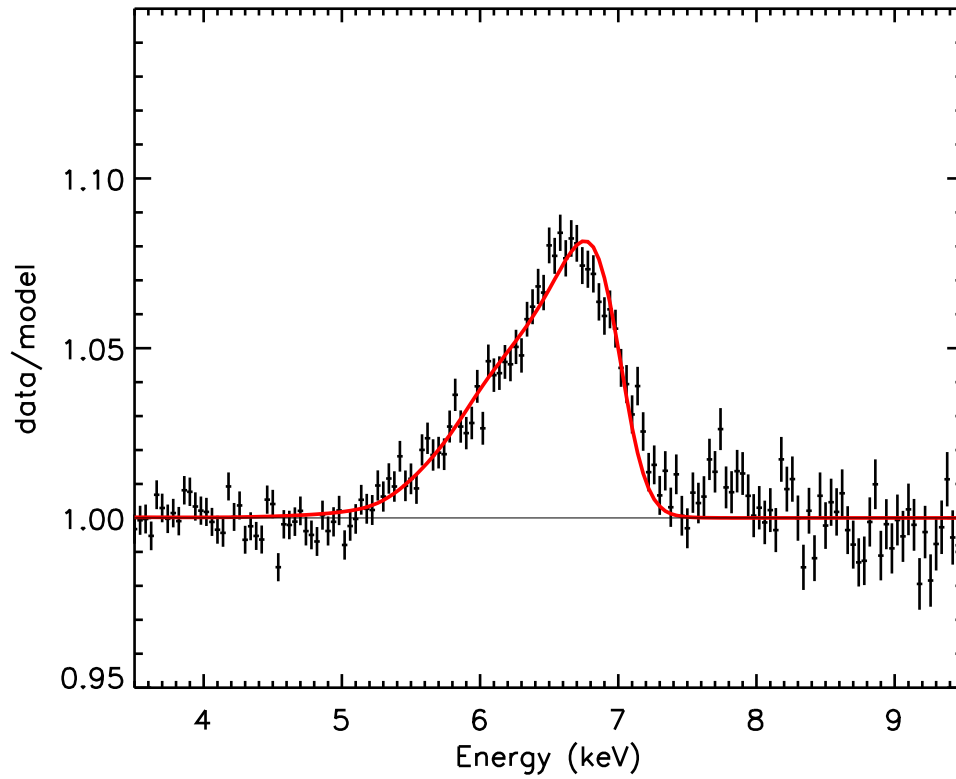FIG. 2.— The relativistic Fe K disk line in the combined FPMA and FPMB spectrum of Serpens X-1 is shown above. The best three–component continuum model was fit over the 3–40 keV band, ignoring the 4.5–7.5 keV range to avoid biasing the continuum fit. The best "kerrdisk" model, derived from fitting the full bandpass including the Fe K region, is shown in red. The spectrum was binned for visual clarity only.

J. M. Miller et al.

TABLE 1
RELATIVISTICALLY-BLURRED DISK REFLECTION MODELS

Spectrum	Model	kT_{disk} (keV)	K_{disk}	kT_{bb} (keV)	K_{bb} (10^{-2})	Γ	K_{pow}	a	q	r_{in} (ISCO)	i (deg.)	ξ (erg cm^{-1})	A_{Fe}	K_{refl} (10^{-11})	χ^2/ν
time-avg	1	1.60(1)	45(2)	2.33(1)	2.52(8)	3.17(3)	1.3(1)	0.0*	2.21(4)	1.2(1)	8^{+2}_{-8}	370(40)	1.0*	4.5(1)	995.1/914
time-avg	2	1.61(3)	44(3)	2.33(2)	2.5(1)	3.18(5)	1.4(2)	0.0*	2.19(3)	1.0*	8^{+2}_{-8}	330(80)	1.0*	5(2)	998.6/915
time-avg.	3	1.61(2)	41(2)	2.33(1)	2.63(6)	3.21(3)	1.5(1)	0.0*	2.26(4)	1.3(1)	8^{+2}_{-8}	220(60)	2.0*	5(2)	962.3/913
time-avg.	4	1.64(3)	41(3)	2.33(2)	2.6(1)	3.22(4)	1.5(1)	0.0*	2.23(3)	1.0*	8^{+2}_{-8}	300(90)	2.0*	6(3)	966.0/915
time-avg.	5	1.64(2)	41(3)	2.33(2)	2.65(5)	3.23(4)	1.5(1)	0.0*	2.29(3)	1.3(1)	8^{+2}_{-8}	200(20)	3.0*	7(2)	950.9/914
time-avg	6	1.64(2)	41(3)	2.33(2)	2.70(5)	3.24(4)	1.6(1)	0.0*	2.27(3)	1.0*	8^{+2}_{-8}	270(90)	3.0*	6(2)	955.9/915
time-avg	7	1.63(3)	42(2)	2.34(1)	2.37(8)	3.21(2)	1.48(3)	0.12*	2.24(4)	1.25(3)	8^{+2}_{-8}	240(30)	1.0*	6.0(9)	998.4/914
time-avg	8	1.61(3)	43(3)	2.33(2)	2.5(1)	3.21(3)	1.5(1)	0.12*	2.20(4)	1.0*	8^{+2}_{-8}	340(90)	1.0*	5(2)	998.7/915
time-avg	9	1.63(2)	41(2)	2.33(1)	2.6(1)	3.21(3)	1.5(1)	0.12*	2.24(4)	1.3(2)	8^{+2}_{-8}	250(60)	2.0*	7(3)	962.4/914
time-avg	10	1.64(3)	41(3)	2.33(2)	2.61(9)	3.23(4)	1.6(2)	0.12*	2.22(3)	1.0*	8^{+2}_{-8}	300(90)	2.0*	6(2)	966.6/915
time-avg	11	1.64(2)	40(1)	2.33(1)	2.69(3)	3.22(2)	1.51(5)	0.12*	2.27(3)	1.35(3)	8^{+2}_{-8}	210(20)	3.0*	6.1(6)	950.9/914
time-avg	12	1.64(3)	40(3)	2.33(2)	2.69(9)	3.24(4)	1.6(2)	0.12*	2.26(3)	1.0*	8^{+8}_{-8}	280(90)	3.0*	5(3)	957.1/915
time-avg	13	1.64(1)	42(2)	2.35(1)	2.5(2)	3.20(2)	1.5(1)	0.14*	2.22(3)	1.4(1)	8^{+2}_{-8}	290(40)	1.0*	5.2(4)	995.8/914
time-avg	14	1.61(3)	44(3)	2.34(2)	2.5(2)	3.19(4)	1.5(2)	0.14*	2.19(3)	1.0*	8^{+4}_{-8}	330(90)	1.0*	5(2)	1000.0/915
time-avg	15	1.63(1)	41(2)	2.33(1)	2.6(1)	3.22(2)	1.47(6)	0.14*	2.25(3)	1.4(1)	8^{+2}_{-8}	220(60)	2.0*	7(2)	962.2/914
time-avg	16	1.64(3)	41(3)	2.33(2)	2.7(2)	3.24(4)	1.6(2)	0.14*	2.23(3)	1.0*	8^{+2}_{-8}	300(90)	2.0*	6(3)	967.6/915
time-avg	17	1.65(1)	41(1)	2.31(3)	2.69(4)	3.20(2)	1.51(4)	0.14*	2.27(3)	1.41(4)	8^{+2}_{-6}	210(30)	3.0*	6(1)	951.0/914
time-avg	18	1.65(2)	41(3)	2.33(1)	2.7(1)	3.25(4)	1.6(2)	0.14*	2.27(3)	1.0*	8^{+8}_{-8}	270(90)	3.0*	5(2)	958.1/915
high-flux	19	1.75(5)	37(3)	2.40(2)	2.6(2)	3.30(5)	1.7(3)	0.00*	2.21(7)	$1.2^{+0.4}_{-0.2}$	8^{+3}_{-8}	380(90)	1.0*	5(2)	936.7/914
high-flux	20	1.73(5)	36(4)	2.49(4)	2.6(2)	3.31(7)	1.8(3)	0.00*	2.21(6)	1.0*	8^{+4}_{-8}	360(80)	1.0*	5(2)	937.1/915
high-flux	21	1.73(6)	36(3)	2.39(3)	2.6(3)	3.35(9)	1.8(3)	0.00*	2.26(6)	$1.1^{+0.4}_{-0.1}$	8^{+3}_{-8}	310(90)	2.0*	6(3)	928.8/914
high-flux	22	1.75(6)	35(5)	2.38(3)	2.6(3)	3.33(7)	1.8(3)	0.00*	2.25(6)	1.0*	8^{+4}_{-8}	330(90)	2.0*	6(3)	929.6/915
high-flux	23	1.73(4)	35(4)	2.38(2)	2.7(2)	3.33(7)	1.8(3)	0.00*	2.31(7)	$1.2^{+0.3}_{-0.2}$	8^{+4}_{-8}	330(90)	3.0*	5(2)	926.4/914
high-flux	24	1.76(6)	34(4)	2.39(4)	2.7(3)	3.35(8)	1.9(4)	0.00*	2.29(5)	1.0*	8^{+5}_{-8}	340(90)	3.0*	6(3	927.5/915

NOTE. — The results of fits with relativistically-blurred disk reflection components ("reflionx" convolved with "kerrconv") are presented here. The disk emissivity is measured by the parameter q ($J\,r^{-q}$). Parameters fixed at a given value are marked with an asterisk. The ionization of the disk is measured by the ionization parameter ξ. All fits were made assuming an equivalent neutral hydrogen column density of $N_H = 4.0 \times 10^{21}\,\mathrm{cm}^{-2}$ as per Dickey & Lockman (1990), via the "tbabs" model. All errors quoted in the table are 1σ uncertainties.
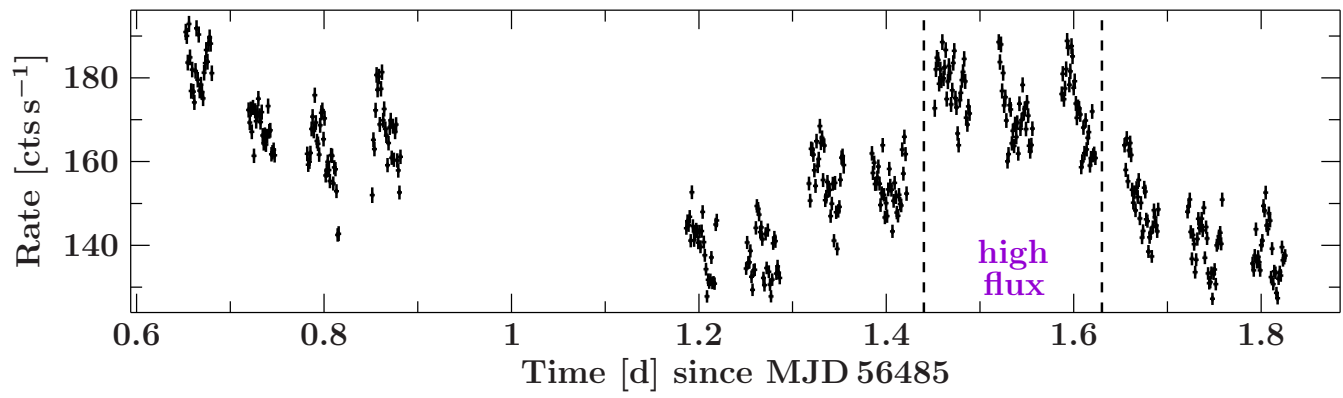
FIG. 3.— The *NuSTAR* light curve of Serpens X-1. The interval defined as "high flux" was selected for independent spectral analysis for comparison (see Table 1).
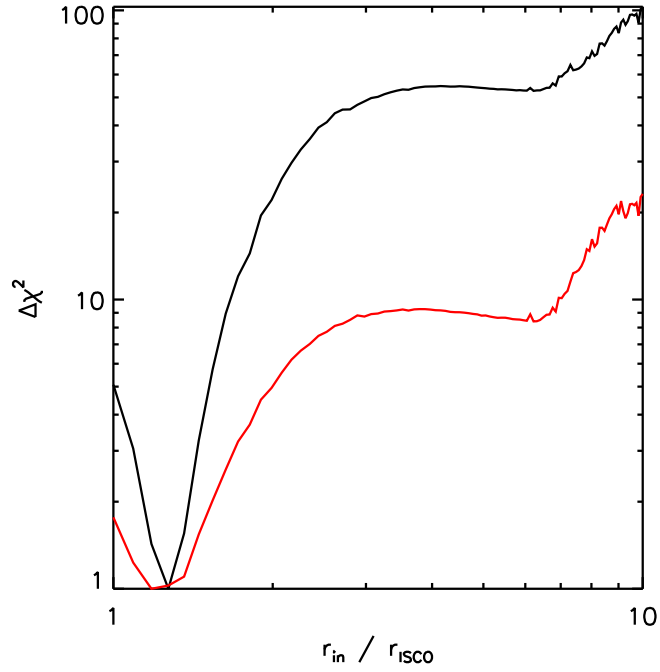
FIG. 4.— The figure above displays the change in the fitting statistic, $\Delta\chi^2$, versus the inner disk radius measured via two blurred reflection fits. Model 5, which is a fit to the time-averages spectrum of Serpens X-1, is shown in black. Model 23, which is a fit to the high-flux phase of the observation (see Section 3), is shown in red. Both models, like others detailed in Table 1, strongly prefer a disk that is close to a likely ISCO, and are statistically consistent with the disk extending to the ISCO itself. For plotting clarity, a constant of 1.0 was added to all $\Delta\chi^2$ values.